

Mapping partial wave dynamics in scattering resonances by rotational de-excitation collisions

Tim de Jongh^{1 *†}, Quan Shuai^{1 *††}, Grite L. Abma¹, Stach Kuijpers¹, Matthieu Besemer¹,
Ad van der Avoird¹, Gerrit C. Groenenboom^{1 **},
Sebastiaan Y.T. van de Meerakker^{1 **}

¹Radboud University, Institute for Molecules and Materials
Heyendaalseweg 135, 6525 AJ Nijmegen, the Netherlands

[†] Present address: Laboratoire Kastler Brossel, ENS-Université PSL,
CNRS, Sorbonne Université, Collège de France, 24 rue Lhomond, 75005 Paris, France

^{††} Present address: State Key Laboratory of Molecular Reaction Dynamics,
Dalian Institute of Chemical Physics, Chinese Academy of Sciences, Dalian, 116023, China.

* Who contributed equally to this work

** To whom correspondence should be addressed

E-mail: basvdm@science.ru.nl, gerritg@theochem.ru.nl

December 15, 2021

Abstract

One of the most important parameters in a collision is the ‘miss distance’ or impact parameter, which in quantum mechanics is described by quantized partial waves. Usually, the collision outcome is the result of unavoidable averaging over many partial waves. Here we present a study of low-energy NO–He collisions, that enables us to probe how individual partial waves evolve during the collision. By tuning the collision energies to scattering resonances between 0.4 and 6 cm⁻¹, the initial conditions are characterized by a limited set of partial waves. By preparing NO in a rotationally excited state before the collision and by studying rotational de-excitation collisions, we were able to add one quantum of angular momentum to the system and trace how it evolves. Distinct fingerprints in the differential cross sections yield a comprehensive picture of the partial wave dynamics during the scattering process. Exploiting the principle of detailed balance, we show that rotational

de-excitation collisions probe time-reversed excitation processes with superior energy and angular resolution.

Understanding the interactions between individual atoms and molecules at the complete quantum level is of fundamental importance to physics and chemistry. Collision experiments have proven an indispensable tool to unravel these interactions. The key to understanding a collision lies with investigating how the interaction potential transforms the reagent states into the product states. Experimentally, this is best probed by so-called state-to-state measurements, in which the initial conditions are precisely controlled and the final conditions are precisely detected. To date, state-to-state measurements for (almost) all degrees of freedom have become possible. Ingenious methods have for instance been developed to prepare a single rotational or vibrational state of a molecule before the collision, and to detect it state-selectively afterwards [1, 2, 3, 4].

In addition to the quantized energy levels of an isolated molecule, quantization also appears when the molecule interacts with another particle. The relative motion of the particles is perceptibly quantized in terms of the orbital angular momentum, labeled by the integer ℓ , which replaces the classical notion of the impact parameter by its quantum mechanical analogue of partial waves. The nomenclature of these discrete orbital states is similar to that of the electronic states of the hydrogen atom: $\ell = 0, 1, 2, \dots$ are named *s*, *p*, *d*, ... waves, respectively.

Gaining control over this relative motion (i.e., impact parameter or partial waves) is a long-standing dream in state-to-state measurements [5]. Indeed, the ultimate information about a collision event would be found by selecting a single partial wave ℓ_{in} from the initial conditions, and by subsequently following how the interaction transforms it into product partial waves ℓ_{out} . Directly probing the transition $\ell_{\text{in}} \rightarrow \ell_{\text{out}}$ poses a tremendous challenge, however, and is in many cases even considered impossible. Herschbach *et al.* affectionately characterized the task of measuring and controlling the impact parameter as the pursuit of the ‘forbidden fruit’ in reaction dynamics [6, 7]. The number of partial waves taking part in a collision event is directly connected to the particles’ de Broglie wavelength, and hence to the temperature or collision energy. The higher the collision energy, the smaller the de Broglie wavelength, and the larger the number of partial waves contributing to the collision. These interfere with each other, which hampers a detailed view on how the interaction potential transforms ℓ_{in} into ℓ_{out} at the single partial wave level.

The main strategy to constrain the number of possible values for ℓ_{in} – and thus to obtain a clear picture of the partial wave evolution during a collision – therefore lies with studying collisions at the lowest possible temperature [8, 3, 2]. In the extreme case where the temperature approaches zero kelvin one enters the ultracold Wigner limit [9]. Here, the de Broglie wavelength approaches infinity and we find a situation where in principle only a single partial wave contributes – for most systems this is the *s*-wave –, unequivocally defining ℓ_{in} . At slightly higher temperatures several incoming partial waves start to contribute to the collision, but effects of single partial waves can often still be traced through scattering resonances. Such a resonance implies that the scattering partners briefly form a quasi-bound state, and that only one – or at most a few – partial wave(s) dominate(s) over other contributing waves. Tuning the collision energy to a scattering resonance therefore offers the opportunity to ‘select’ a single partial wave from the initial conditions. This strategy works best at energies just above the ultracold Wigner

regime, where the number of partial waves is still low such that scattering resonances appear as prominent and distinct features in the cross sections.

Although spectacular progress has recently been made to experimentally study molecular collisions at ever lower energies — fully resolving scattering resonances and even approaching the Wigner limit — [8, 3, 2, 10, 11, 12, 13, 14, 15, 16], there are still caveats for studying the evolution of partial waves during a collision event. In the ultracold regime the de Broglie wavelength becomes so large that the topology of the underlying interaction potential becomes irrelevant. Integral scattering cross sections (ICSs) simply obey the universal Wigner laws, and the differential cross sections (DCSs) show no intrinsic structure. In the resonance regime, cross sections do possess intrinsic structure related to the dominating partial wave, but so little energy is available that the exit channel is necessarily governed by the same ‘selected’ initial partial wave and little is learnt about the *evolution* of partial waves [16]. In addition, typically only a very limited number of collision channels are energetically open, restricting the information that can be harvested from the potential across its entire energy landscape. Both effects pose a fundamental dilemma for experiments designed to probe the collision dynamics at the state-to-state partial wave level: The energy regime in which individual partial waves are most easily probed, is also the energy regime in which one becomes insensitive to how the interaction potential transforms these waves during a collision.

Here we present a strategy that resolves this catch-22, and that allows us to experimentally probe the transition $\ell_{\text{in}} \rightarrow \ell_{\text{out}}$ in the cleanest way. To this end, we exploit a degree of freedom of molecules that is foreign to atoms: rotational motion. The key idea is to probe collisions in the translationally cold Wigner or low-energy resonance regime such that the entrance channel is dominated by a single partial wave only, and to add well-defined quanta of angular momentum by rotationally exciting the molecules prior to the collision. The study of rotational de-excitation collisions makes it possible to trace how this additional amount of angular momentum is transferred into translational motion. The outgoing de Broglie wavelength is substantially decreased, which enriches the spectrum of outgoing partial waves. The released kinetic energy has the additional experimental benefit of increasing the otherwise minute collisional recoil energies, making it easier to resolve structures in the DCS. Last but not least, the pre-collision excitation allows for a larger number of energetically allowed collision channels, offering more sensitive probes of the interaction potential.

Experimental studies on rotational de-excitation collisions at low energies largely remain unexplored territory. In photodissociation of ultracold molecules — where an additional quantum of angular momentum is offered by a photon — similar ideas have previously been exploited to probe partial wave dynamics [3, 8]. For rotational state-to-state experiments such ideas were previously explored theoretically [17], whereas recent measurements of collisions involving rovibrationally excited NO molecules demonstrated the possibility of monitoring rotational de-excitation in low-energy collisions [18]. However, the relatively high energies involved in that study obscured clear resonance structures and the partial wave fingerprints underlying the collisions.

We studied collisions between NO radicals and He atoms in a crossed molecular beam

machine. By optically preparing rotationally excited NO radicals prior to the collision, we measured scattering resonances in the ICSs and DCSs for rotational de-excitation collisions with energies between 0.4 and 6 cm^{-1} and an energy resolution up to 0.07 cm^{-1} . By tuning the collision energy to individual resonances, the observed structures in the DCSs revealed how the additional quantum of rotational energy transforms into the quantized relative motion of the recoiling collision partners, revealing state-to-state energy transfer at the full partial wave level. In addition, exploiting the principle of detailed balance, we demonstrate that measurements of rotational de-excitation processes provide a way to probe the time-reversed inelastic excitation processes with much improved energy resolution. Moreover, inelastic de-excitation processes do not have the energy threshold of the corresponding excitation processes, which allows us to measure resonance effects in cross sections at even lower energies. Our results are in good agreement with state-of-the-art quantum chemistry calculations at the CCSDT(Q) level.

Results and Discussion

Low energy scattering resonances

Low-energy rotational de-excitation collisions between He atoms and NO molecules were studied in a crossed molecular beam machine that combines Stark deceleration and velocity map imaging (VMI) [19, 20]. The NO molecules were state-selected and velocity controlled by the Stark decelerator and subsequently excited into the $X^2\Pi_{1/2}, \nu = 1, j = 3/2, f$ state by a quantum cascade laser (QCL). Here, $X^2\Pi_{1/2}, \nu$ and j indicate the electronic, vibrational and rotational states, respectively and each rotational state is split into two Λ -doublet components of opposite parity indicated by the labels e and f . In the following we will drop the electronic state label $X^2\Pi_{1/2}$ and use the subscripts ‘in’ and ‘out’ to indicate angular momentum quantum numbers for the reagents and products. Rovibrational excitation of the NO radicals using the infrared radiation offered by a QCL was chosen over a pure rotational transition (which would require a THz source) for experimental reasons. The induced vibrational excitation generally does not influence the scattering process and the vibrational motion can in most cases be regarded a spectator in the collision process (see Supplementary section 1.3).

We measured state-to-state ICSs for the $\nu = 1, j_{\text{in}} = 3/2, f \rightarrow \nu = 1, j_{\text{out}} = 1/2, f$ and $\nu = 1, j_{\text{in}} = 3/2, f \rightarrow \nu = 1, j_{\text{out}} = 1/2, e$ rotational de-excitation channels of NO at energies between 0.4 and 6 cm^{-1} . We refer to these de-excitation transitions as channels A and B, and present the results in Figures 1a and 1b, respectively. An energy level diagram indicating the involved rovibrational states and collision induced transitions is presented in Figure 1c. The experimentally obtained ICSs are compared with theoretical predictions based on a state-of-the-art interaction potential created with the coupled cluster method involving single, double, triple and perturbative quadruple excitations [CCSDT(Q)], as described in Ref. [16]. These theoretical curves were convoluted with a Gaussian of varying width to account for the experimental energy resolution, which ranged from 0.07 cm^{-1} at the lowest energy to 0.4 cm^{-1}

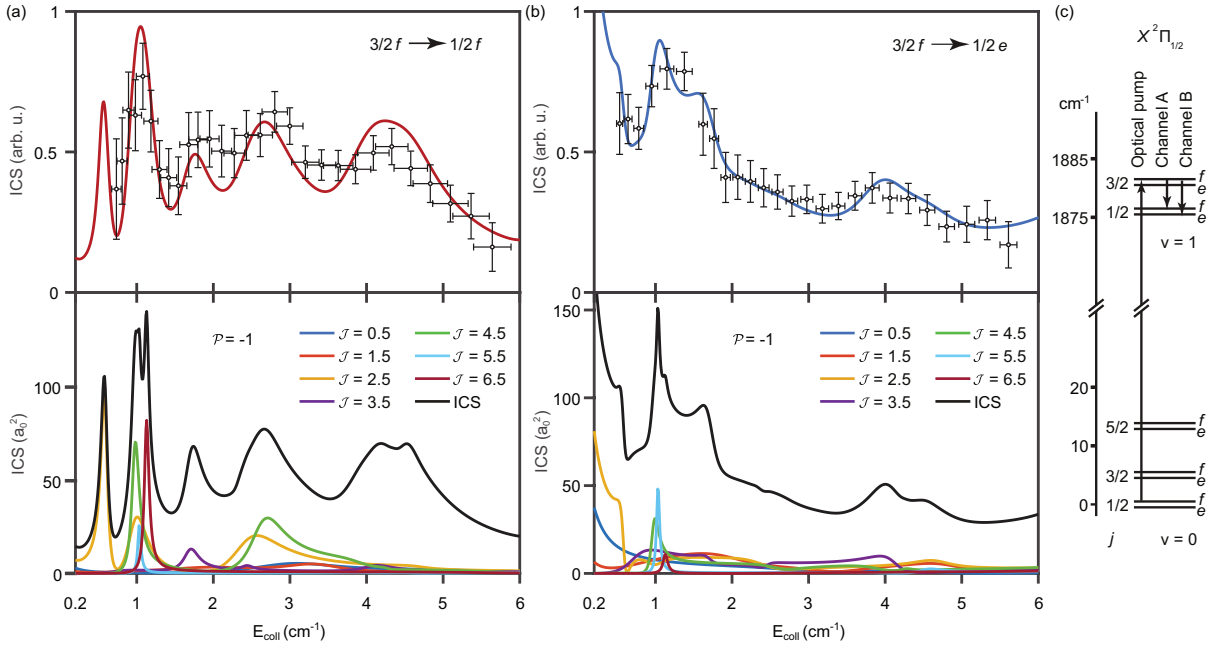


Figure 1: Collision energy dependence of the ICS and energy level diagram of the involved molecular states. Comparison between measured (data points with error bars) and calculated (solid curves) state-to-state inelastic scattering cross sections for the (a) $\nu = 1, j_{\text{in}} = 3/2, f \rightarrow \nu = 1, j_{\text{out}} = 1/2, f$ and (b) $\nu = 1, j_{\text{in}} = 3/2, f \rightarrow \nu = 1, j_{\text{out}} = 1/2, e$ transitions. Experimental data is given in arbitrary units (arb. u.). Vertical error bars display statistical uncertainties at 95% of the confidence interval. Horizontal error bars represent the uncertainty in energy calibration. Solid lines show the theoretical curves convoluted with experimental energy spread (upper panels, overlay with data points), and individual partial wave contributions to the cross sections for $\mathcal{P} = -1$ (lower panels). (c) Energy level diagram of $\text{NO}(X^2\Pi_{1/2})$, indicating the optical transition used to prepare NO radicals in the $\nu = 1, j = 3/2, f$ state (upward arrow), and the collision induced rotational de-excitation transitions studied (downward arrows). Energy level splittings due to Λ -doubling are greatly exaggerated for clarity.

at the highest energy. Experimental data points are vertically scaled using root-mean-square fitting and corrected for density-to-flux effects. For both channels, the measured ICS shows good agreement with theoretical calculations, with peaks clearly indicating the presence of partial wave resonances.

To investigate the nature of these resonances, we decomposed the theoretically predicted cross sections in terms of the conserved total angular momentum quantum number \mathcal{J} and overall parity $\mathcal{P} = \pm 1$. Figures 1a and 1b show the individual partial wave contributions for $\mathcal{P} = -1$, which largely dominate the resonance structures (see Supplementary section 2.1). The resonances are seen to be relatively pure and are dominated by only a few values for \mathcal{J} .

The purity of the strong resonance feature in the $\nu = 1, j_{\text{in}} = 3/2, f \rightarrow \nu = 1, j_{\text{out}} = 1/2, f$ channel just below 1 cm^{-1} is near-ideal, and is governed by only one value for \mathcal{J} . Due to the conservation of \mathcal{J} and \mathcal{P} , the values for the partial wave quantum numbers ℓ_{in} and ℓ_{out} are constrained by the initial j_{in} and final j_{out} rotational states of NO — taking the vector addition of angular momenta into account — via (see Supplementary section 2.2):

$$\vec{\mathcal{J}} = \vec{j}_{\text{in}} + \vec{\ell}_{\text{in}} = \vec{j}_{\text{out}} + \vec{\ell}_{\text{out}}, \quad (1)$$

and

$$\mathcal{P} = \epsilon_{\text{in}}(-1)^{j_{\text{in}}-1/2+\ell_{\text{in}}} = \epsilon_{\text{out}}(-1)^{j_{\text{out}}-1/2+\ell_{\text{out}}}, \quad (2)$$

where ϵ equals $+1$ and -1 for rotational states with labels e and f , respectively.

Both rotational de-excitation transitions probed here ensure $\Delta j = j_{\text{out}} - j_{\text{in}} = -1$, resulting in a richer evolution from ℓ_{in} to ℓ_{out} compared to previous low-energy NO-He experiments that were restricted by $\Delta j = 0$ [16]. Furthermore, they offer the additional benefit of a broader and more sensitive probe of the interaction potential. Channels A and B connect rotational levels with identical quantum numbers j_{in} and j_{out} , but different values for ϵ . Parity changing and parity conserving transitions are governed by different expansion terms of the interaction potential [21], and their joint study yields a more complete picture of the interaction than measurements of the single $j_{\text{in}} = 1/2, f \rightarrow j_{\text{out}} = 1/2, e$ transition that is available without pre-excitation (see Supplementary section 2.4). For channels A and B, from application of equations 1 and 2 we can derive the propensity rules for the partial wave quantum number $\Delta\ell = \pm 1$ and $\Delta\ell = 0, \pm 2$, respectively, where $\Delta\ell > 0$ generally has the largest contribution to the cross sections (see Supplementary section 2.3).

Figure 2 illustrates the relation between \mathcal{J} , ℓ_{in} and ℓ_{out} for channel A at collision energies of $0.5, 1.1, \text{ and } 2.0 \text{ cm}^{-1}$, i.e., at energies around the first three prominent scattering resonances occurring for this transition. It is seen that de-excitation collisions add one unit to the partial wave quantum number, consistent with the propensity rule $\Delta\ell = 1$. At 0.5 cm^{-1} , a single total angular momentum value dominates ($\mathcal{J} = 5/2$) causing the incoming p -waves ($\ell_{\text{in}} = 1$) to be almost fully converted into outgoing d -waves ($\ell_{\text{out}} = 2$). This low energy resonance exquisitely illustrates the advantage of measuring rotational de-excitation processes to probe partial wave dynamics in collisions: The purity of the incoming p -wave can only be achieved at energies approaching the ultracold regime, while the introduction of outgoing partial waves with higher ℓ is only allowed because of the released quantum of angular momentum stored in the rotation of the incoming NO molecule. A similar analysis was made for the resonances observed in channel B (see Supplementary Information), where the evolution of partial waves was found to follow the propensity rule $\Delta\ell = 0$ or 2 .

Evolution of partial waves

The evolution of partial waves $\ell_{\text{in}} \rightarrow \ell_{\text{out}}$ in a collision event is directly encoded in the measured DCS, which reflects the outgoing partial waves, each corresponding to a spherical harmonic of

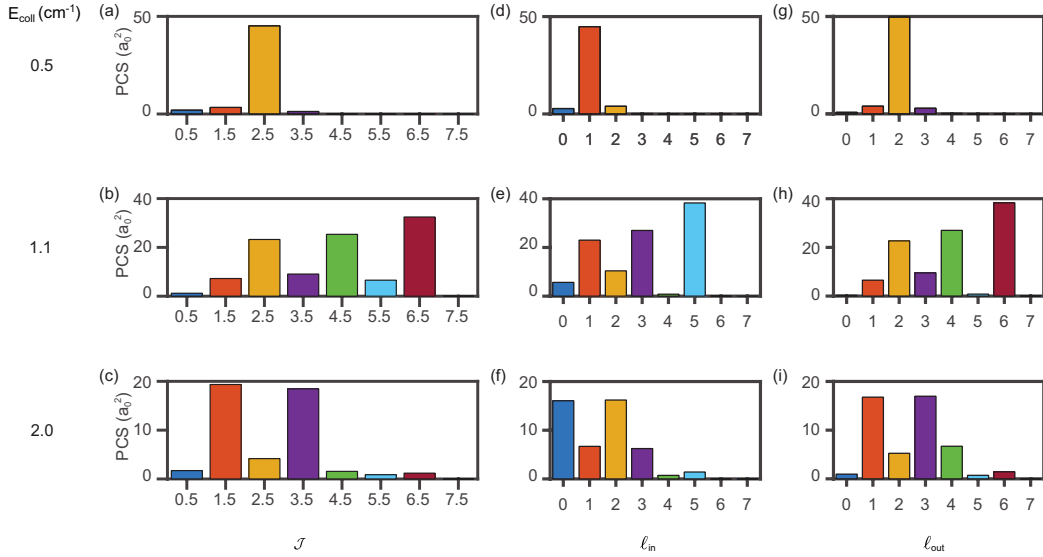


Figure 2: Theoretically predicted partial cross section (PCS) contributions for the total angular momentum \mathcal{J} (a-c) as well as the incoming (ℓ_{in}) (d-f) and outgoing (ℓ_{out}) partial wave (g-i) for the $\nu = 1, j_{\text{in}} = 3/2, f \rightarrow \nu = 1, j_{\text{out}} = 1/2, f$ rotational de-excitation channel at three collision energies close to a scattering resonance. Experimental energy spreads ($\Delta E_{\text{coll}}=0.08, 0.19, 0.28 \text{ cm}^{-1}$ (FWHM) for $E_{\text{coll}} = 0.5, 1.1, 2.0 \text{ cm}^{-1}$, respectively) have been taken into account.

degree ℓ_{out} . The number of nodes in the DCS is related with the largest value of ℓ_{out} [22], leading to an isotropic pattern in the case of pure s -wave scattering, a pattern with at most a single node for pure p -wave scattering, and so on. We therefore probed DCSs for both collision induced $\Delta j = -1$ de-excitation transitions by measuring velocity mapped ion images at several selected collision energies between 0.4 and 2.0 cm^{-1} . To elucidate the effect of the additional quantum of angular momentum released in the de-excitation collision, we compared our results with measurements from $\Delta j = 0$ transitions. To this end, we measured ion images for the previously [16] investigated $\nu = 0, j_{\text{in}} = 1/2, f \rightarrow \nu = 0, j_{\text{out}} = 1/2, e$ parity de-excitation channel at the same collision energies. Effects of the difference in vibrational state exist but in most cases were small enough to warrant direct comparison and trace the effects of the released quantum of angular momentum in the rotational de-excitation channels (Supplementary section 1.3).

The experimentally obtained ion images are shown in Figure 3 for each scattering channel and collision energy. In these images, the angular distribution reflects the underlying DCS. Indeed, the distributions for $\Delta j = -1$ rotational de-excitation transitions show more complex features with additional nodes compared to the $\Delta j = 0$ transition, a direct consequence of the transition of rotational into translational angular momentum. The rotational de-excitation

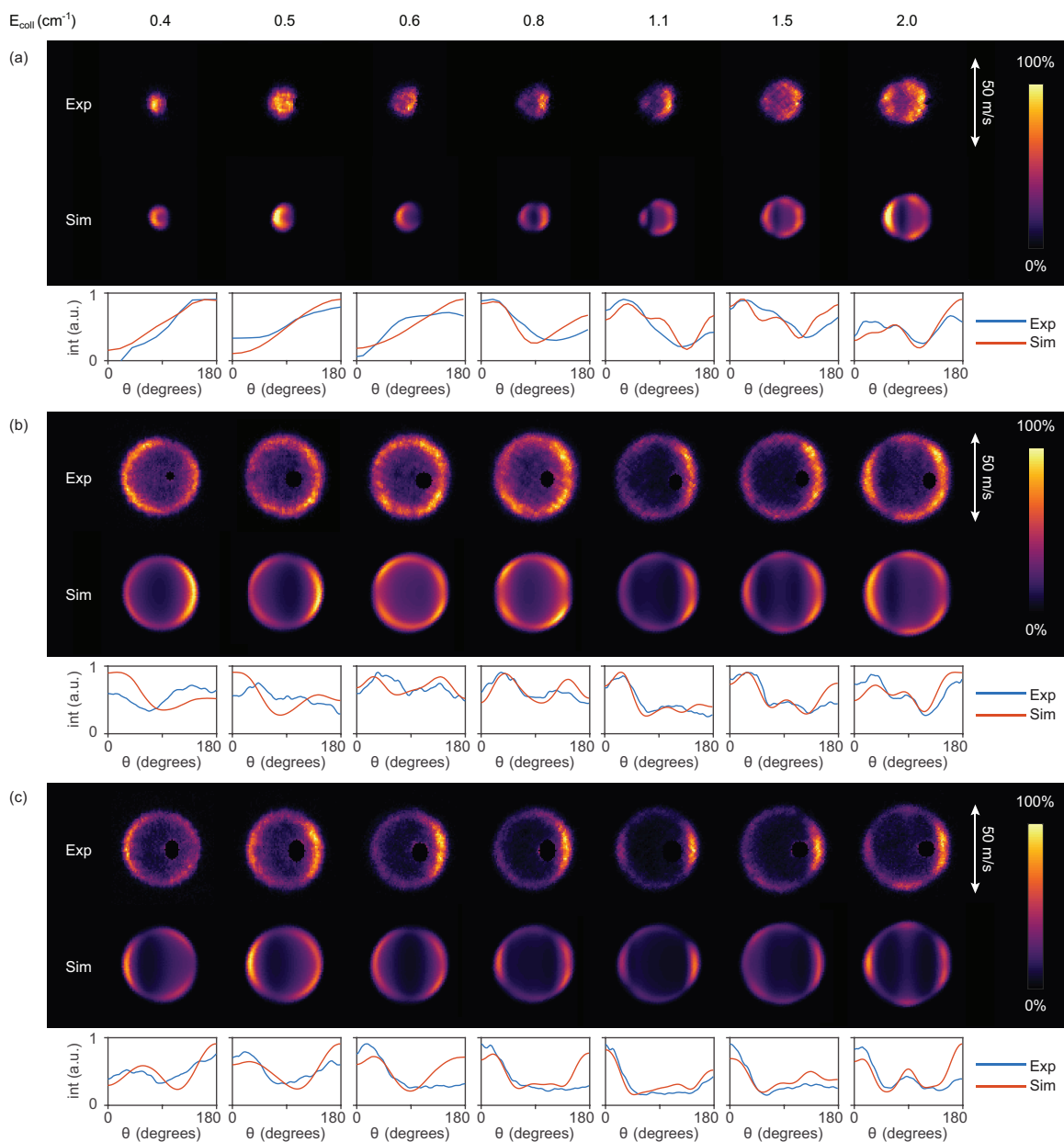


Figure 3: Experimental and simulated ion images at selected collision energies for the (a) $\nu = 0, j_{\text{in}} = 1/2 f \rightarrow \nu = 0, j_{\text{out}} = 1/2 e$ parity de-excitation collisions, (b) $\nu = 1, j_{\text{in}} = 3/2, f \rightarrow \nu = 1, j_{\text{out}} = 1/2, e$ rotational de-excitation channel, and the (c) $\nu = 1, j_{\text{in}} = 3/2, f \rightarrow \nu = 1, j_{\text{out}} = 1/2, f$ rotational de-excitation channel. Collision energies are indicated in the top of the figure and are identical throughout each column. Experimental (Exp) and simulated (Sim) ion images are rotated such that the relative velocity vector is oriented horizontally, with the forward scattering direction on the right side of each image. Color scale represents intensity and the overall intensity scale for the simulated images is fitted to that of the experiment. A small portion of the images is masked due to imperfect state selection of the incoming NO molecules. Angular distributions are extracted from the ion images and plotted for each channel and collision energy.

channels furthermore lead to distinctly larger ion images than the $\Delta j = 0$ parity de-excitation channel as a result of the transfer of internal into kinetic energy. This enables a higher resolution in the measured angular distributions of the scattering products. In addition, the scattering signal is well separated from the image position of the reagent packet, referred to as the beam spot, which is caused by imperfect state selection of the reagent beam and is masked in the images by a black spot. Simulations of the expected images based on DCSs computed with the CCSDT(Q) potential are shown as well, together with the angular distributions extracted from both the experimental and simulated images. These simulations take the full kinematics of the experiment into account, such as collision energy spreads and detection efficiencies. Overall, good agreement is obtained between theory and experiment, although for channel A disparities are found in the backward scattering region ($\theta \approx 180^\circ$) at 0.6 and 0.8 cm^{-1} . We speculate that this may be due to the strongly varying DCS across this energy range near the steep rising edge of a resonance.

The increased complexity of the DCS structure caused by the added quantum of angular momentum can be directly related to the evolution of partial waves during the collision. This can be seen most clearly at the lowest energies probed. Here, the $\Delta j = 0$ channel displays a rather simple angular distribution, consistent with the interference of only *s*- and *p*-wave distributions found at these energies [16]. By contrast, the $\Delta j = 1$ rotational de-excitation transitions measured at the same collision energy lead to structures with a larger number of nodes, indicative for the additional contributions of outgoing waves with $\ell_{\text{out}} > \ell_{\text{in}}$ and consistent with the propensity rules for the partial waves discussed above. Specifically, for channel A at $E_{\text{coll}} = 0.5 \text{ cm}^{-1}$ — which exhibits the most pristine partial wave resonance probed here — the observed two-node structure in the angular distribution directly reveals the evolution of a *p*-wave into a *d*-wave that underlies the scattering event.

Detailed balance

The DCS measurements presented in Figure 3 thus display many advantages introduced by adding an internal quantum of angular momentum before the collision. Yet there is another aspect that can be exploited to study low-energy collision phenomena: owing to the principle of time-reversal invariance, de-excitation collisions probe the same partial wave dynamics that underlies the corresponding excitation process, but with a significantly higher experimental energy resolution. This principle — often also referred to as the principle of microscopic detailed balance [23, 24] — dictates that the DCS for a scattering event is identical to the DCS for the time-reversed process apart from a constant factor, with time-reversal effectively swapping $(j_{\text{in}}, \ell_{\text{in}})$ and $(j_{\text{out}}, \ell_{\text{out}})$ (see Supplementary sections 2.5 and 2.6), provided that the total (kinetic + rotational) energy remains the same. Whereas the excitation process has an energetic threshold corresponding to the internal energy of the excited state, de-excitation processes can be probed at arbitrarily low energies where the experimental energy resolution is typically much higher.

The experimental arrangement used here, which offers access to well-resolved scattering

resonances and the possibility to prepare molecules in a rotationally excited state, yields the unique opportunity to probe two complementary time-reversed processes under similar circumstances. To illustrate this, we compared the scattering images for the $\nu = 1, j_{\text{in}} = 3/2, f \rightarrow \nu = 1, j_{\text{out}} = 1/2, f$ de-excitation channel at collision energies E_{coll} (from Figure 3) with images taken for the $\nu = 0, j_{\text{in}} = 1/2, f \rightarrow \nu = 0, j_{\text{out}} = 3/2, f$ excitation transition at energies $E_{\text{coll}} + \Delta E_{\text{rot}}$, where $\Delta E_{\text{rot}} = 5.02 \text{ cm}^{-1}$ is the energy difference between the $j = 1/2$ and $j = 3/2$ rotational states of NO. Under these conditions, we can regard these transitions as each other’s time-reversed process for which the reversibility principle should hold, provided that the vibrational state is a spectator in the collision process. From theoretical calculations, we found that in most cases the effects from the difference in vibrational states can indeed be neglected (see Supplementary section 1.3).

The images pertaining to the $j_{\text{in}} = 3/2 \rightarrow j_{\text{out}} = 1/2$ de-excitation channel from the last row of Figure 3 are re-plotted for selected energies in Figure 4, together with the obtained ion images for the corresponding $j_{\text{in}} = 1/2 \rightarrow j_{\text{out}} = 3/2$ excitation channel. For both channels, the simulated images and extracted angular distributions are shown as well. The ion images for the $j_{\text{in}} = 1/2 \rightarrow j_{\text{out}} = 3/2$ excitation channel show two concentric rings, with the smaller ring pertaining to the $\nu = 0, j_{\text{in}} = 1/2, f \rightarrow \nu = 0, j_{\text{out}} = 3/2, f$ transition and the larger ring caused by elastic collisions involving NO radicals in the $\nu = 0, j = 3/2, f$ state, which is present in minute amounts in the primary NO packet. This outer ring appears as a relatively strong feature due to the much larger cross section for elastic scattering compared to inelastic collisions.

Overall, good agreement is obtained between the experimental and the simulated images. However, at the lower energies probed the angular distributions of the de-excitation and its time-reversed excitation process appear rather different, seemingly violating the principle of detailed balance. Yet, the purely theoretical DCSs (within the respective vibrational states) underlying these simulated images are shown in the rightmost column of Figure 4, and are found to be indeed identical, except at a collision energy of 1.1 cm^{-1} (6.1 cm^{-1} for the excitation channel) in the vicinity of a scattering resonance, where the vibration causes a notable difference in the cross sections (Supplementary section 1.3). This apparent contradiction is merely a direct consequence of the kinematics of the experiment: The higher collision energy for the excitation process results in a larger collision energy spread, and the transfer of kinetic into rotational energy results in a smaller image. Both have substantial consequences for the observable angular distribution in a scattering image: The larger energy spread causes averaging of the cross sections within a broader energy range, while structures in the DCS are more easily blurred in images with small diameter. These effects are taken into account in the simulations, and cause the angular distributions of the simulated scattering images to deviate, even though the underlying DCSs obey detailed balance.

These results further underline that by virtue of time-reversal invariance, rotational excitation processes are actually probed with superior energy and angular resolution by measuring the corresponding de-excitation channel instead. For the energy ranges investigated here, the collision energy spread (FWHM) for the de-excitation collisions ranges from 0.07 to 0.3 cm^{-1}

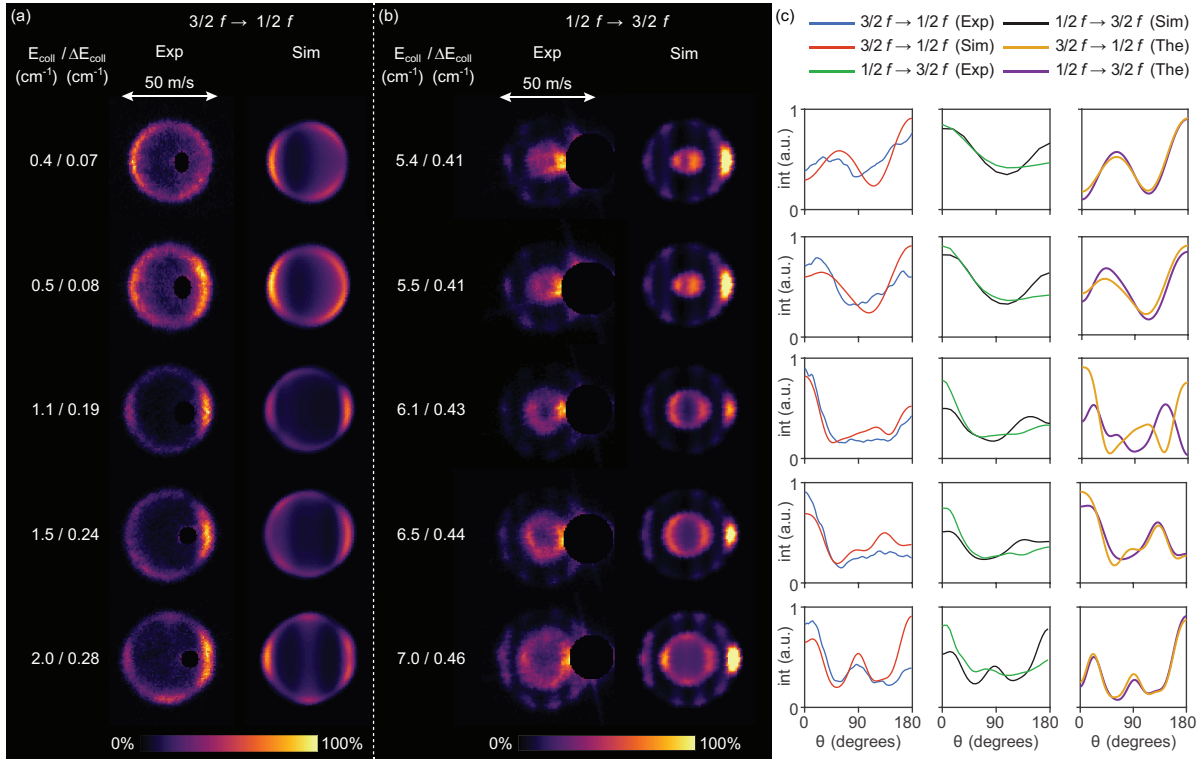


Figure 4: Experimental (Exp) and simulated (Sim) ion images for two inelastic scattering processes subject to the detailed balance principle. (a) Images for the $\nu = 1, j_{\text{in}} = 3/2, f \rightarrow \nu = 1, j_{\text{out}} = 1/2, f$ rotational de-excitation process at selected collision energies E_{coll} . (b) Images for the $\nu = 0, j_{\text{in}} = 1/2, f \rightarrow \nu = 0, j_{\text{out}} = 3/2, f$ rotational excitation channel at energies $E_{\text{col}} + \Delta E_{\text{rot}}$, with $\Delta E_{\text{rot}} = 5 \text{ cm}^{-1}$. The experimental collision energy spread ΔE_{coll} is indicated for each image. An outer ring is visible that is caused by elastic scattering of NO molecules in the $\nu = 0, j = 3/2, f$ state. Part of the forward scattering direction of these outer rings are masked due to imperfect state selection of the NO radicals. Images are oriented such that the relative velocity vector is aligned horizontally, with the forward direction on the right. (c) Extracted angular distributions for the inelastic channels plotted for each collision energy as well as normalized purely theoretical DCSs (The) within the respective vibrational states.

whereas it ranges from 0.41 to 0.44 cm⁻¹ for the excitation collisions. At the lowest energies probed, this enhancement in resolution can thus reach up to a factor 5 or higher. Furthermore, the larger image diameter afforded by the de-excitation measurements translates into an angular resolution of approximately 3°, whereas the angular resolution of the excitation images is between 5°-18°.

Conclusion

The study of low-energy molecular collisions provides unique opportunities to trace the partial wave dynamics underlying a scattering event. The limited set of incoming partial waves available at these energies is a prerequisite for the mapping of their dynamics, but the typically equally limited set of outgoing partial waves reduces the sensitivity to the interaction potential. Using rovibrational excitation of the reagent molecules, and subsequently studying de-excitation inelastic scattering, we were able to resolve this catch-22 as it introduces an additional available quantum of angular momentum to the outgoing spectrum of partial waves. We traced its effects on the scattering dynamics by measuring integral and differential cross sections at energies in the vicinity of scattering resonances, revealing the evolution of partial waves throughout the scattering process. Furthermore, the larger number of energetically accessible inelastic collision channels afforded by the pre-collision excitation offered more detailed probes of the interaction potential across its entire energy landscape. Rotational de-excitation collisions were also demonstrated to offer superior resolution — in both the collision energy and the angular distribution of the scattering products — compared to their time-reversed rotational excitation counterparts. Optical excitation of reagent molecules to any initial rotational state can in principle be achieved by sequential rotational excitations, offering the unique opportunity to study how controlled amounts of angular momentum stored in translationally ultracold molecules is released at the full partial wave level.

Acknowledgements

This work is part of the research program of the Netherlands Organization for Scientific Research (NWO). S.Y.T.v.d.M. acknowledges support from the European Research Council (ERC) under the European Union’s Seventh Framework Program (FP7/2007-2013/ERC Grant Agreement No. 335646 MOLBIL) and from the ERC under the European Union’s Horizon 2020 Research and Innovation Program (Grant Agreement No. 817947 FICOMOL). We thank N. Janssen and A. van Roij for expert technical support. We thank F.J.M. Harren for stimulating discussions regarding the optical excitation of NO using a quantum cascade laser. We thank Tijs Karman for fruitful discussions and for critically reading the manuscript.

Author Contributions

The project was conceived by S.Y.T.v.d.M. The experiments were carried out by T.d.J., Q.S. and S.K.. Methods to rovibrationally excite NO using a quantum cascade laser were developed by G.A. and Q.S.. Data analysis and simulations were performed by T.d.J. Theoretical calculations were performed by M.B., A.v.d.A. and G.C.G. The manuscript was written by T.d.J. and S.Y.T.v.d.M. with contributions from all authors. All authors were involved in the interpretation of the data and the preparation of the manuscript.

Competing Interest Statement

There are no competing interests.

References

- [1] Chadwick, H., Hundt, P. M., van Reijzen, M. E., Yoder, B. L. & Beck, R. D. Quantum state specific reactant preparation in a molecular beam by rapid adiabatic passage. *J. Chem. Phys.* **140**, 034321 (2014).
- [2] Perreault, W. E., Mukherjee, N. & Zare, R. N. Quantum control of molecular collisions at 1 Kelvin. *Science* **358**, 356 (2017).
- [3] McDonald, M. *et al.* Photodissociation of ultracold diatomic strontium molecules with quantum state control. *Nature* **535**, 122 (2016).
- [4] Hu, M.-G. *et al.* Direct observation of bimolecular reactions of ultracold KRb molecules. *Science* **366**, 1111–1115 (2019).
- [5] Herschbach, D. R. Molecular dynamics of elementary chemical reactions (nobel lecture). *Angew. Chem. Int. Ed.* **26**, 1221–1243 (1987).
- [6] Herschbach, D. Chemical stereodynamics: retrospect and prospect. *The European Physical Journal D* **38**, 3–13 (2006).
- [7] Anggara, K., Leung, L., Timm, M. J., Hu, Z. & Polanyi, J. C. Approaching the forbidden fruit of reaction dynamics: Aiming reagent at selected impact parameters. *Science Advances* **4**, eaau2821 (2018).
- [8] Volz, T. *et al.* Feshbach spectroscopy of a shape resonance. *Physical Review A* **72**, 010704(R) (2005).
- [9] Wigner, E. P. On the behavior of cross sections near thresholds. *Phys. Rev.* **73**, 1002–1009 (1948).
- [10] Jankunas, J., Jachymski, K., Hapka, M. & Osterwalder, A. Observation of orbiting resonances in He(³S₁) + NH₃ Penning ionization. *J. Chem. Phys.* **142**, 164305 (2015).
- [11] Klein, A. *et al.* Directly probing anisotropy in atom–molecule collisions through quantum scattering resonances. *Nat. Phys.* **13**, 35 (2017).
- [12] Lavert-Ofir, E. *et al.* Observation of the isotope effect in sub-kelvin reactions. *Nat. Chem.* **6**, 332–335 (2014).
- [13] Bergeat, A. *et al.* Understanding the quantum nature of low-energy C (³P_{*j*}) + He inelastic collisions. *Nat. Chem.* **10**, 519 (2018).
- [14] Bergeat, A., Onvlee, J., Naulin, C., van der Avoird, A. & Costes, M. Quantum dynamical resonances in low-energy CO (*j* = 0) + He inelastic collisions. *Nat. Chem.* **7**, 349 (2015).

- [15] Bergeat, A., Morales, S. B., Naulin, C., Wiesenfeld, L. & Faure, A. Probing low-energy resonances in water-hydrogen inelastic collisions. *Phys. Rev. Lett.* **125**, 143402 (2020).
- [16] de Jongh, T. *et al.* Imaging the onset of the resonance regime in low-energy NO-He collisions. *Science* **368**, 626–630 (2020).
- [17] Onvlee, J., van der Avoird, A., Groenenboom, G. & van de Meerakker, S. Y. T. Probing scattering resonances in (ultra)cold inelastic NO–He collisions. *The Journal of Physical Chemistry A* **120**, 4770–4777 (2016).
- [18] Amarasinghe, C. *et al.* State-to-state scattering of highly vibrationally excited NO at broadly tunable energies. *Nat. Chem.* **12**, 528–534 (2020).
- [19] van de Meerakker, S. Y. T., Bethlem, H. L., Vanhaecke, N. & Meijer, G. Manipulation and control of molecular beams. *Chem. Rev.* **112**, 4828–4878 (2012).
- [20] Eppink, A. T. J. B. & Parker, D. H. Velocity map imaging of ions and electrons using electrostatic lenses: Application in photoelectron and photofragment ion imaging of molecular oxygen. *Rev. Sci. Instrum.* **68**, 3477–3484 (1997).
- [21] Aoiz, F. J. *et al.* Inelastic scattering of He atoms and NO($X^2\Pi$) molecules: The role of parity on the differential cross section. *The Journal of Physical Chemistry A* **113**, 14636–14649 (2009).
- [22] *NIST Handbook of Mathematical Functions Paperback and CD-ROM* (Cambridge University Press, Cambridge, UK, 2010).
- [23] Boltzmann, L. Weitere Studien über das Wärmegleichgewicht unter Gasmolekülen. *Wien. Ber.* **66**, 275–370 (1872).
- [24] Einstein, A. Strahlungs-Emission und - Absorption nach der Quantentheorie. *Verhandlungen der Deutschen Physikalischen Gesellschaft* **18**, 318–323 (1916).

Methods

The experiments were performed in a crossed-molecular beam apparatus described previously [1]. A supersonic beam of 5% NO seeded in Kr or Ar was expanded through a Nijmegen Pulsed Valve [2] and subsequently entered a 2.6 m long Stark decelerator. The resulting NO molecules in the $X^2\Pi_{1/2}, \nu = 0, j = 1/2, f$ state were velocity selected with a mean velocity between 480 and 720 m/s and a longitudinal spread of approximately 2.1 m/s (1σ). At a distance of 5 mm from the exit of the Stark decelerator these molecules were rovibrationally excited by a distributed feedback QCL (Thorlabs, QD5316CM) at a wavelength of approximately 5.3 μm , inducing the $\nu' = 1, j' = 3/2, f, F' = 5/2 \leftarrow \nu'' = 0, j'' = 1/2, f, F'' = 3/2$ transition in

order to obtain the highest yield of excited NO radicals (see Supplementary section 1.2). Here F indicates the initial and final total angular momentum including nuclear spin. The nuclear spin can be treated as a spectator as well [3], which was verified by studying rotational inelastic collisions when inducing other hyperfine transitions (see Supplementary section 1.2).

The packet of NO radicals intercepted a neat beam of He under an angle of 5° . This secondary beam was expanded through a commercially available Even-Lavie Valve [4] which was cooled by a cryogenic cold head to temperatures between 15 K and 30 K, resulting in He velocities between 460 and 575 m/s. Calibration of the He velocity and the energy resolution was performed by measuring a previously identified resonance peak in the $\nu = 0, j_{\text{in}} = 1/2, f \rightarrow \nu = 0, j_{\text{out}} = 1/2, e$ channel of NO-He collisions near a collision energy of 1 cm^{-1} [1]. Scattered NO radicals were state-selectively detected using $1+1'$ resonance enhanced multiphoton ionization involving the (1-1) band of the $A^2\Sigma^+ \leftarrow X^2\Pi_{1/2}$ transition using two dye lasers pumped by a single Nd:YAG laser. The ions were then mapped onto a microchannel plate using an advanced velocity map imaging spectrometer yielding a resolution of 0.8 m/s/pixel [5].

For DCS measurements, a small image correction — a 5 % compression of the image in the vertical direction — was made to mitigate the effect of slight distortions expected to be caused by the presence of external magnetic fields. ICS measurements were performed with the imaging spectrometer out of focus in order to avoid detector saturation. The collision energy was tuned by scanning the NO velocity between 580 and 720 m/s using the Stark decelerator. In order to obtain optimal resolution [6], we measured two energy ranges separately using different He velocities (approximately 480 and 550 m/s). Results were corrected for beam density and flux-to-density effects. Details on the simulations are given elsewhere [7].

References

- [1] de Jongh, T. *et al.* Imaging the onset of the resonance regime in low-energy NO-He collisions. *Science* **368**, 626–630 (2020).
- [2] Yan, B. *et al.* A new high intensity and short-pulse molecular beam valve. *Rev. Sci. Instrum.* **84**, 023102 (2013).
- [3] Ball, C. D. & De Lucia, F. C. Direct observation of Λ -doublet and hyperfine branching ratios for rotationally inelastic collisions of NO - He at 4.2 K. *Chem. Phys. Lett.* **300**, 227–235 (1999).
- [4] Even, U. Pulsed supersonic beams from high pressure source: Simulation results and experimental measurements. *Adv. Chem.* **2014**, 636042 (2014).
- [5] Plomp, V., Gao, Z. & van de Meerakker, S. Y. T. A velocity map imaging apparatus optimised for high-resolution crossed molecular beam experiments. *Mol. Phys.* **119**, e1814437 (2021).

- [6] Scharfenberg, L., van de Meerakker, S. Y. T. & Meijer, G. Crossed beam scattering experiments with optimized energy resolution. *Phys. Chem. Chem. Phys.* **13**, 8448 (2011).
- [7] von Zastrow, A. *et al.* State-resolved diffraction oscillations imaged for inelastic collisions of NO radicals with He, Ne and Ar. *Nat. Chem.* **6**, 216–221 (2014).